

Supporting information

Highly Luminescent Nanoscale Quasi-2D Layered Lead Bromide Perovskites with Tunable Emissions

Zhao Yuan,^a Yu Shu,^a Yan Xin,^b and Biwu Ma^{a,c,d}*

*^a Department of Chemical and Biological Engineering, FAMU-FSU College of
Engineering, Tallahassee, FL 32310, USA*

*^b National High Magnetic Field Laboratory, Florida State University, Tallahassee, FL
32310, USA*

^c Materials Science Program, Florida State University, Tallahassee, FL 32306, USA

*^d Department of Chemistry and Biochemistry, Florida State University, Tallahassee, FL
32306, USA*

Table of contents

- (a) Materials
- (b) Synthesis of the quasi-2D layered nanoperovskites
- (c) Characterization methods
- (d) AFM images of the NPs
- (e) ^1H NMR spectra of the NPs
- (f) TGA analysis of the NPs
- (g) The schematic layered quasi-2D structures of NPs
- (h) Composition of the components in the NPs.
- (i) The summary of the XRD analyses
- (j) Acknowledgement

(a) Materials

Lead(II) bromide (99.999%), methylamine solution (33 wt. % in absolute ethanol), octylamine (99%), benzylamine (99%), octadecylamine (99%) and hydrobromic acid (48%) were purchased from Sigma-Aldrich. Acetone (99.5%) was purchased from VWR. *N,N*-Dimethylformamide (99.9%), toluene (99.9%) and hexane (98.5%, mixture of isomers) were purchased from Sigma-Aldrich. All reagents and solvents were used without further purification unless otherwise stated. Spectroscopic grade solvents were used in the UV-Vis and photoluminescence spectroscopic measurements.

(b) Synthesis of the quasi-2D layered nanoperovskites

The organic ammonium bromide salts were prepared by adding slightly excess hydrobromic acid solution (48%) into the corresponding amines, respectively, in ethanol at 0 °C. The ammonium salts were obtained after removal of the solvents and starting reagents under vacuum, followed by washing with ethyl ether by three times, after which the ammonium bromides were dried and kept in a desiccator for future use.

A typical procedure of making the quasi-2D layered nanoperovskites is described as follow: 0.1 mmol lead(II) bromide (0.10 mmol, 36.7 mg) was dissolved in 200 μ L DMF and mixed with 33.6 mg octylammonium bromide (0.16 mmol) and 11.2 mg methylammonium bromide (0.10 mmol) in 100 μ L DMF to form a clear precursor solution (300 μ L DMF in total), which was subsequently dropped into 2 mL hexanes with vigorously stirring for 5 min at room temperature. The corresponding NPs were induced right after the addition of 3 mL acetone followed by centrifugation to remove the unreactive materials in the supernatant, affording the final products in a decent yield after dried under vacuum. The different amounts of the organic ammonium bromides used for each products are summarized in Table S1.

(c) Characterization methods

Nuclear magnetic resonance (¹H-NMR). ¹H NMR spectra were acquired at room temperature on Bruker AVANCE III NMR Spectrometers with a 500 MHz Bruker magnet. All chemical shifts (δ) were reported in ppm relative to tetramethylsilane (TMS).

Thermogravimetry analysis (TGA). TGA was carried out using a TA instruments Q50 TGA system. The samples were heated from room temperature (~ 22 °C) to 800 °C with at a rate of 5 °C·min⁻¹, under a nitrogen flux of 100 mL·min⁻¹.

X-ray powder diffraction (XRPD). The XRD analysis was performed on Panalytical X'PERT Pro Powder X-Ray Diffractometer using Copper X-ray tube (standard) radiation at a voltage of 40 kV and 40 mA, and X'Celerator RTMS detector. The diffraction pattern was scanned over the angular range of 5-70 degree (2θ) with a step size of 0.02, at room temperature.

Transmission Electron Microscopy images (TEM). Microstructural characterization was performed using transmission electron microscopy (TEM), on a JEOL JEM-ARM200cF at 200kV. Low intensity illumination and fast acquisition time were used during data collection to avoid beam damage. TEM samples were prepared by depositing a few drops of the perovskite solution on a carbon film supported copper grid (200 mesh); the samples were subsequently dried overnight.

Atomic Force Microscopy images (AFM). AFM measurements were conducted using Bruker Icon. All measurements were performed in the standard tapping mode with OTESPA-R3 tips from Bruker.

UV-visible measurements. UV-Vis spectra were conducted at room temperature using a quartz spectrometer cuvette on a Varian Cary 100 Bio UV-Visible spectrophotometer.

Photoluminescence steady state studies. Steady-state photoluminescence spectra were obtained at room temperature on a Varian Cary Eclipse Fluorescence spectrophotometer. All the data were acquired using a 1-cm semi-micro quartz cuvette. The emission spectra of the perovskites dispersed in toluene were measured under air atmosphere (unless otherwise indicated).

Photoluminescence quantum efficiencies. For photoluminescence quantum efficiency measurement, the samples were excited at 360 nm. Absorbance at the excitation wavelength was kept below 0.1 to minimize the inner-filter effect. The fluorescence quantum yields were determined by comparing the integrated area of the corrected emission spectrum with that of the reference – quinine bisulfate ($\phi = 0.54$ in 1 N H_2SO_4).¹

1. S. Fery-Forgues and D. Lavabre, *J. Chem. Ed.*, 1999, **76**, 1260-1264.

(d) AFM images of the NPs

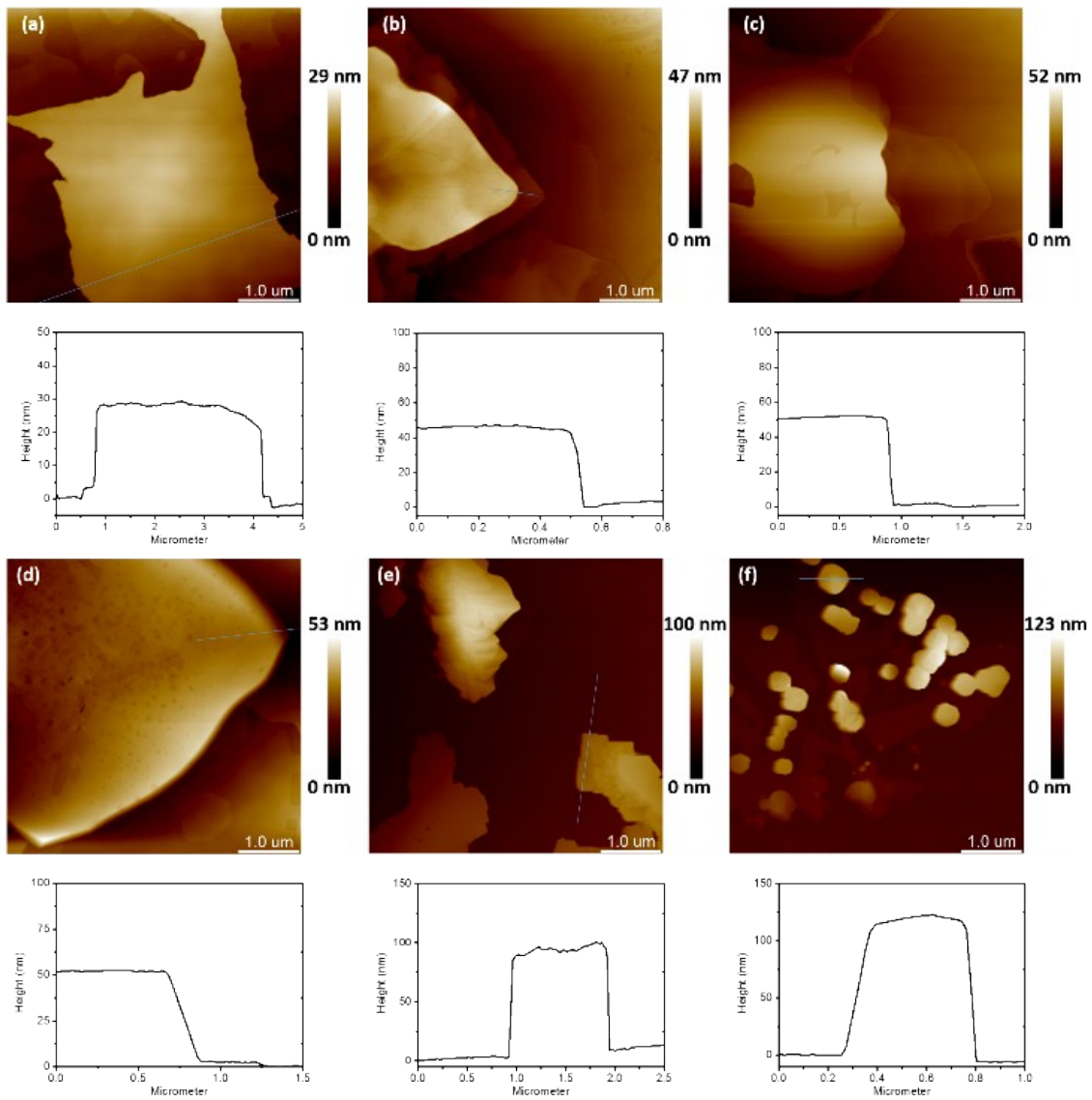


Figure S1. AFM images of NP403 (a); NP442 (b); NP461 (c); NP499 (d); NP513 (e) NP530

(e) ^1H NMR spectra of the NPs

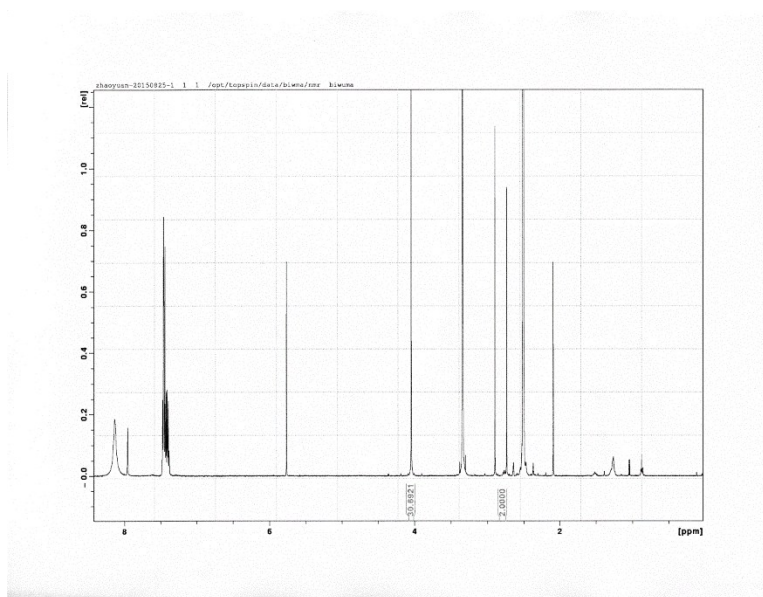


Figure S2. ^1H NMR spectrum of NP403 in DMSO-d_6 .

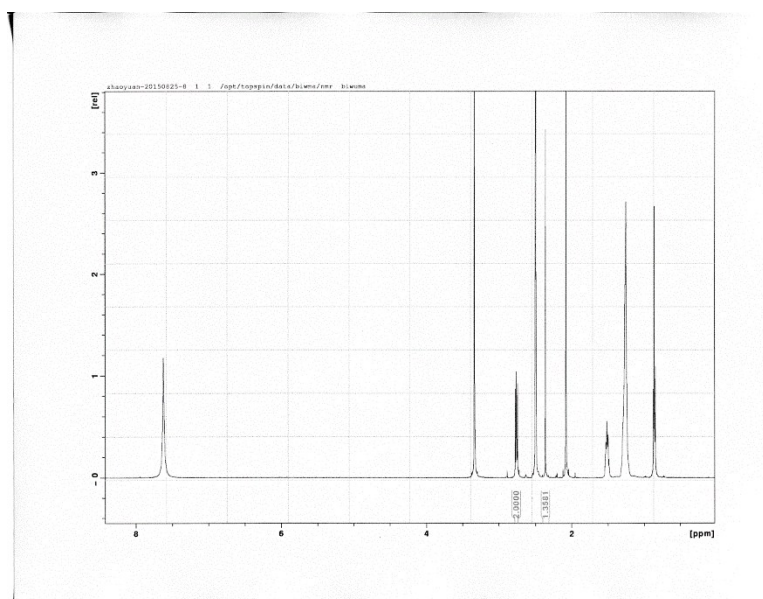


Figure S3. ^1H NMR spectrum of NP442 in DMSO-d_6 .

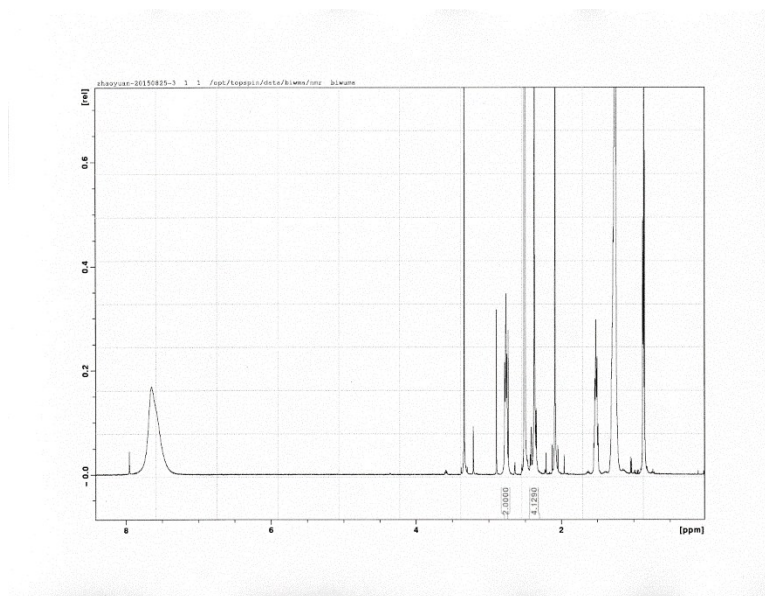


Figure S4. ^1H NMR spectrum of NP461 in DMSO-d_6 .

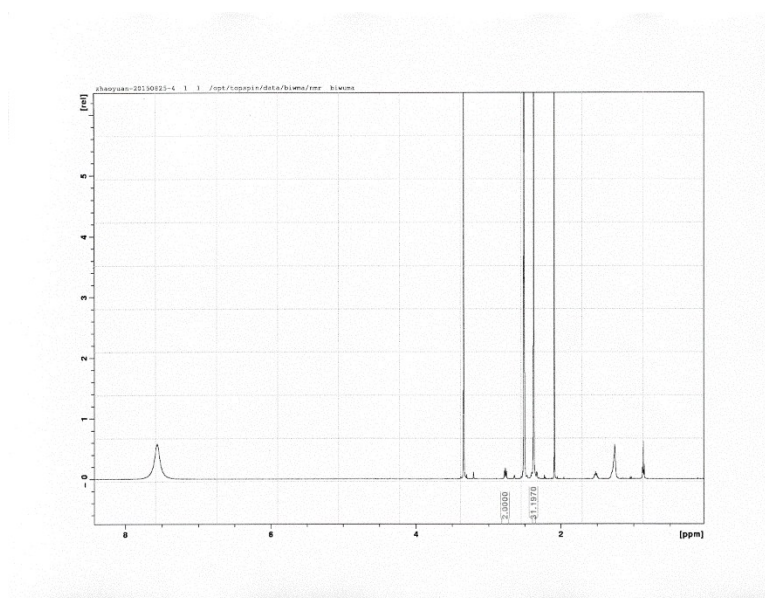


Figure S5. ^1H NMR spectrum of NP499 in DMSO-d_6 .

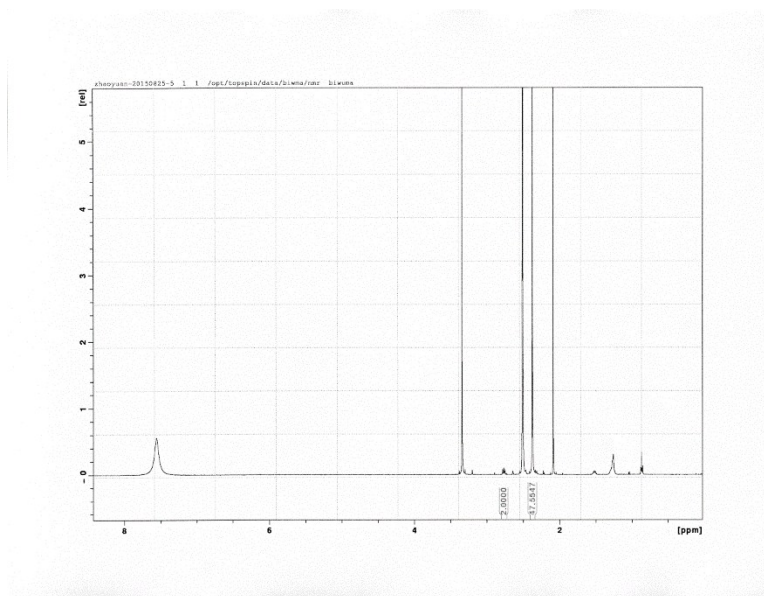


Figure S6. ^1H NMR spectrum of NP513 in DMSO-d_6 .

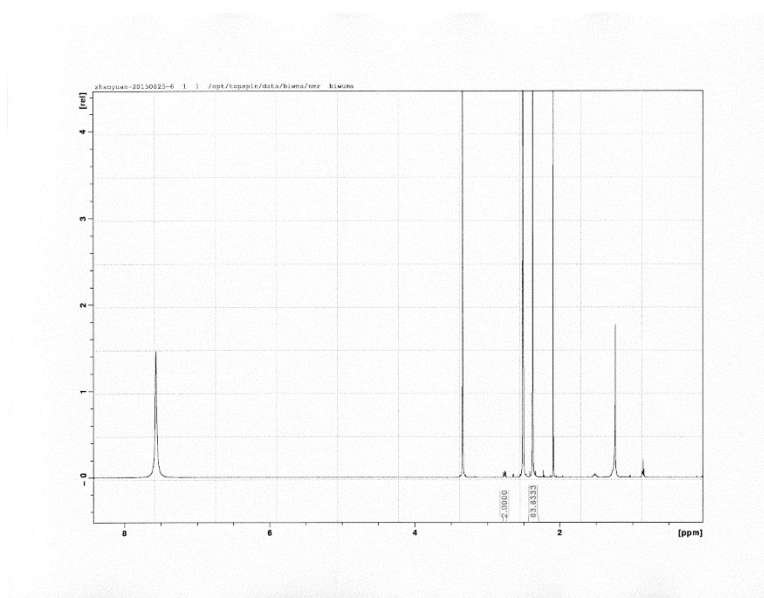


Figure S7. ^1H NMR spectrum of NP530 in DMSO-d_6 .

(f) TGA analysis of the NPs

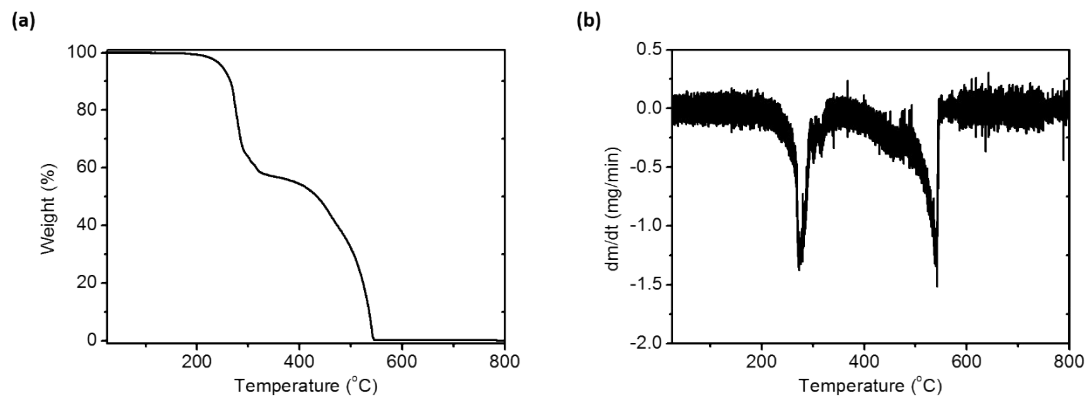


Figure S8. (a) TGA heating curves of NP403. (b) The corresponding 1st derivative.

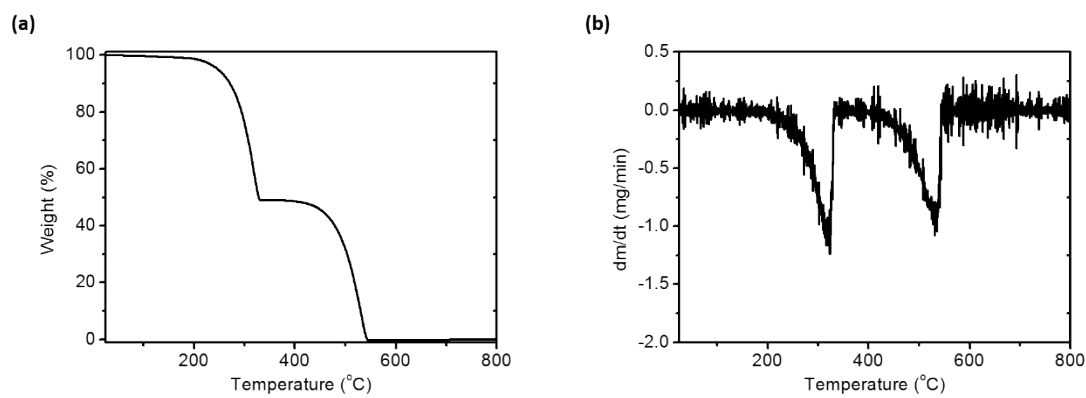


Figure S9. (a) TGA heating curves of NP442. (b) The corresponding 1st derivative.

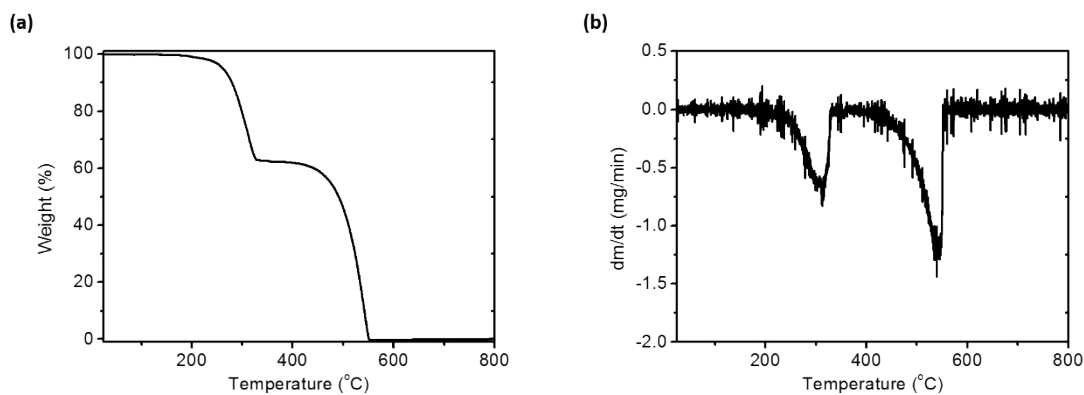


Figure S10. (a) TGA heating curves of NP461. (b) The corresponding 1st derivative.

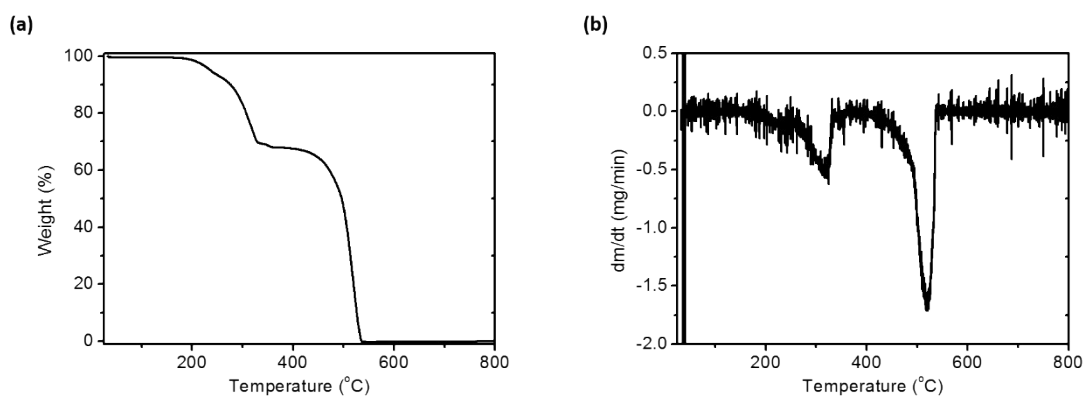


Figure S11. (a) TGA heating curves of NP499. (b) The corresponding 1st derivative.

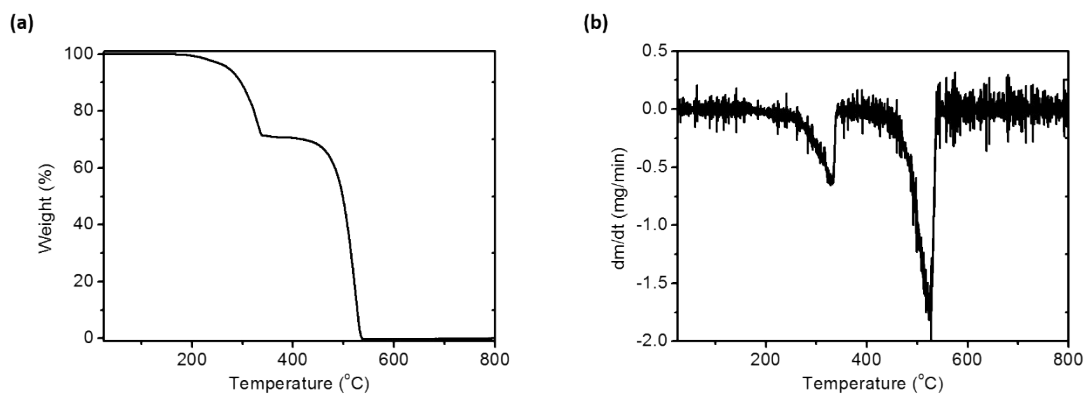


Figure S12. (a) TGA heating curves of NP513. (b) The corresponding 1st derivative.

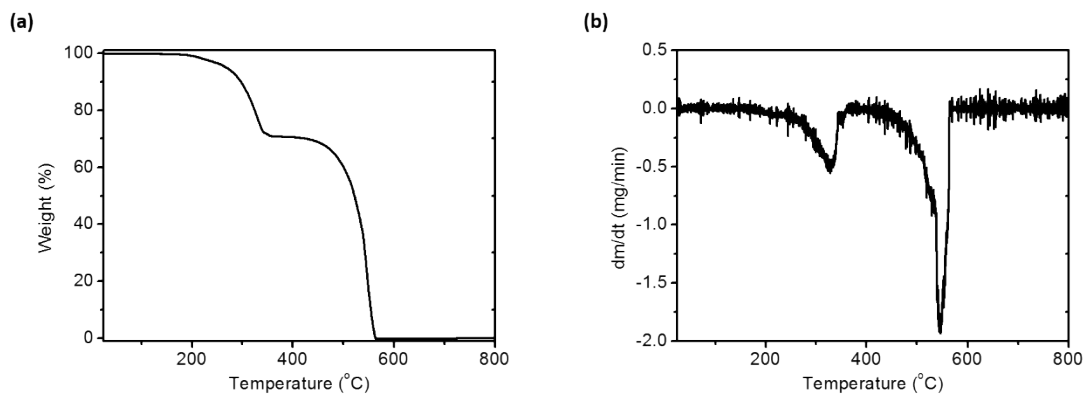


Figure S13. (a) TGA heating curves of NP530. (b) The corresponding 1st derivative.

(g) The schematic layered quasi-2D structures of NPs

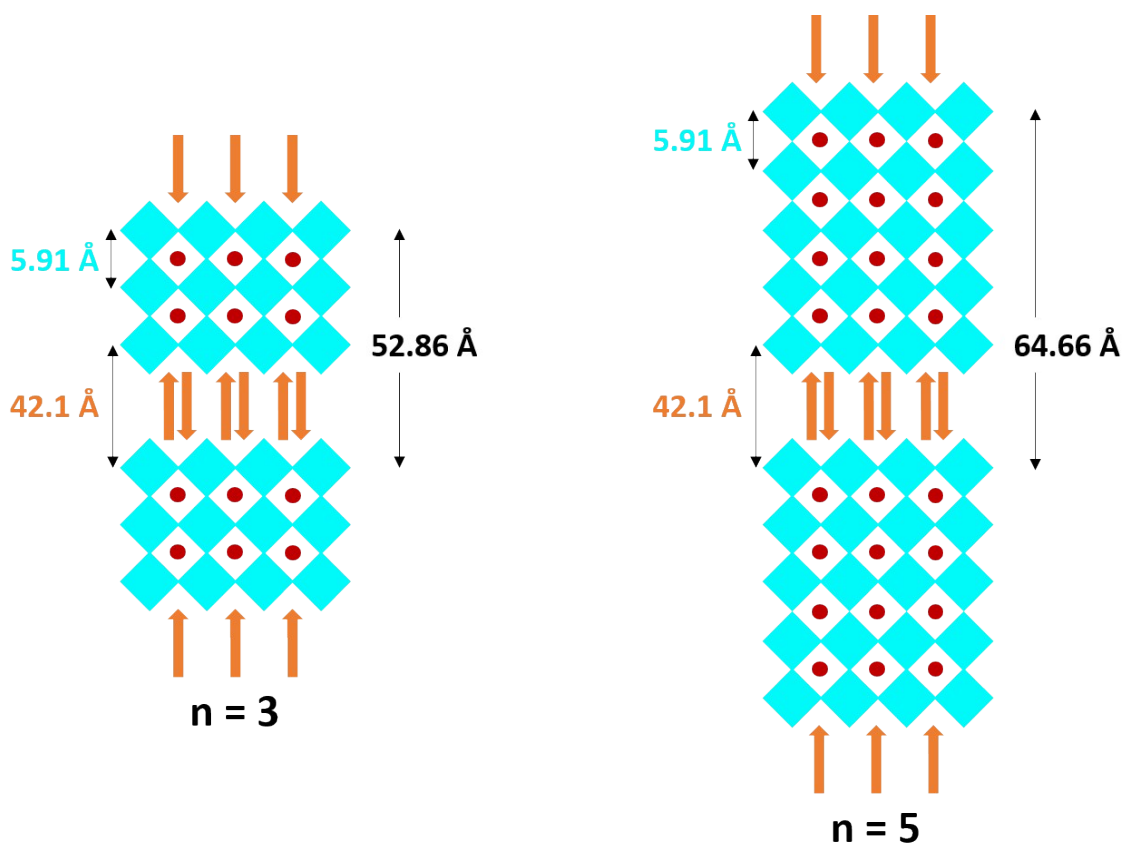


Figure S14. The schematic layered quasi-2D structures of perovskites ($n=3$ and $n=5$).

(h) Table S1. Composition of the components in the NPs according to TGA and ^1H NMR.

Product	Reagent	Starting amount / mmol	Molar ratio ^a	Calculated ratio ^b	Chemical yield ^c
NP403	$\text{C}_8\text{H}_{17}\text{NH}_3\text{Br}$	0.16	0.12	0.22	76 %
	$\text{C}_6\text{H}_5\text{CH}_2\text{NH}_3\text{Br}$	0.24	1.82	1.78	
	PbBr_2	0.10	1.00	1.00	
NP442	$\text{C}_8\text{H}_{17}\text{NH}_3\text{Br}$	0.20	1.46	0.67	74 %
	$\text{CH}_3\text{NH}_3\text{Br}$	0.05	0.66	0.67	
	PbBr_2	0.10	1.00	1.00	
NP461	$\text{C}_8\text{H}_{17}\text{NH}_3\text{Br}$	0.16	0.59	0.40	72 %
	$\text{CH}_3\text{NH}_3\text{Br}$	0.10	0.81	0.80	
	PbBr_2	0.10	1.00	1.00	
NP499	$\text{C}_8\text{H}_{17}\text{NH}_3\text{Br}$	0.07	0.11	0.18	75 %
	$\text{CH}_3\text{NH}_3\text{Br}$	0.20	1.11	0.91	
	PbBr_2	0.10	1.00	1.00	
NP513	$\text{C}_8\text{H}_{17}\text{NH}_3\text{Br}$	0.05	0.07	0.12	76 %
	$\text{CH}_3\text{NH}_3\text{Br}$	0.20	1.12	0.94	
	PbBr_2	0.10	1.00	1.00	
NP530	$\text{C}_{18}\text{H}_{37}\text{NH}_3\text{Br}$	0.01	0.04	0.06	75 %
	$\text{CH}_3\text{NH}_3\text{Br}$	0.20	1.18	0.97	
	PbBr_2	0.10	1.00	1.00	

^a Calculated from the TGA and ^1H NMR results, and based on the mol of PbBr_2 ; ^b Calculated from the XRD and AFM results, and based on the chemical formula of $(\text{RNH}_3)_2(\text{CH}_3\text{NH}_3)_{n-1}\text{Pb}_n\text{Br}_{3n+1}$; ^c Calculated from the TGA results, and based on the weight of PbBr_2 in the nanoperovskites compared to the weight of PbBr_2 used in the reaction (starting amount).

(i) Table S2. The summary of the XRD analyses including miller index, 2θ degree and lattice spaces (d).

NPs	(h k l)	2θ degree	d (Å)
NP403	(0 0 2)	5.29	16.67
	(0 0 4)	10.58	8.34
	(0 0 6)	15.93	5.54
	(0 0 8)	21.26	4.15
	(0 0 10)	26.66	3.31
	(0 0 12)	32.16	2.75
	(0 0 14)	37.66	2.35
NP442	(0 0 6)	10.02	8.81
	(0 0 8)	13.36	6.61
	(0 0 10)	16.73	5.27
	(0 0 12)	20.13	4.39
	(0 0 14)	23.50	3.76
	(0 0 16)	26.93	3.28
	(0 0 18)	30.39	2.91
	(0 0 20)	33.85	2.61
NP461	(0 0 8)	10.92	8.08
	(0 0 10)	13.68	6.45
	(0 0 12)	16.45	5.37
	(0 0 14)	19.22	4.59
	(0 0 16)	22.02	4.01
	(0 0 18)	24.87	3.55
	(0 0 20)	27.58	3.20
	(0 0 22)	30.42	2.90
	(0 0 24)	33.30	2.65
NP499	(0 0 1)	14.88	5.93
	(0 0 2)	30.08	2.94
NP513	(0 0 1)	14.88	5.93
	(0 1 1)	21.13	4.18
	(0 0 2)	30.07	2.94
	(0 1 2)	33.71	2.62
NP530	(0 0 1)	14.87	5.94
	(0 0 2)	30.04	2.94

(j) Acknowledgement.

The authors thank the Florida State University for financial support through the Energy and Materials Initiative. Part of the work was performed at the TEM facility at the National High Magnetic Field Laboratory, which is supported by the FSU Research Foundation, the National High Magnetic Field Laboratory (NSF-DMR-0654118), and the State of Florida. The authors also acknowledge Dr. Lei Zhu for providing access to fluorescence spectrophotometer.